ToF-SIMS Studies of Sulfuric Acid Hydrate Films

John S. Fletcher,[†] Alex Henderson,[†] Andrew B. Horn,[‡] and John C. Vickerman*[,†]

Department of Chemistry, UMIST, Sackville St. Manchester M60 1QD, United Kingdom and Department of Chemistry, University of Manchester, Oxford Road, Manchester M13 9PL, United Kingdom

Received: October 24, 2003; In Final Form: March 4, 2004

A variety of sulfuric acid hydrate films, formed by the co-deposition of SO_3 and H_2O on a cooled substrate, have been analyzed using time-of-flight secondary ion mass spectrometry (ToF-SIMS). The films were produced using procedures developed in recent infrared spectroscopic studies. Spectra have been shown to consist of a series of identifiable fragments, the change in intensities of which can be related to changes in temperature and the relative abundance of H_2O during the deposition of the film under UHV conditions. Depth profiling of the films shows clear evidence of separate surface species on some films and supports the existence of surface molecular hydrates over a stable bulk hydrate film.

Introduction

This report details the application of ToF-SIMS to the study of atmospherically relevant sulfuric acid hydrates by means of a laboratory study of thin films as mimics for atmospheric particulates.

Sulfate particulates and aerosols are produced naturally through volcanic eruption and also as a result of anthropogenic activity, especially biomass burning and the combustion of fossil fuels. The particles can act as condensation nuclei for polar stratospheric clouds (PSCs) or in the aerosol form as additional surfaces for heterogeneous reactions.[1−3] Because PSC nuclei are considered to be mixtures of water and acid (nitric and/or sulfuric), the interaction of atmospheric species with these acid hydrates is of great importance to the partitioning of oxygen/ozone.[4−6] Sulfuric acid hydrates exist predominantly in the lower stratosphere and upper troposphere regions of the atmosphere. There has been considerable interest in reactions on and in such particles,[7−11] although research has not provided the depth of information available on pure ice surfaces.

Under tropospheric conditions, the particles exist as aerosols. Temperature and humidity determine both the acid content of the aerosol as well as particle size.

To understand the heterogeneous reactions occurring in the atmosphere, it is useful to perform controlled laboratory-based experiments on thin-film mimics. Various methods have been employed to generate sulfuric acid-based films over a range of temperatures. In this investigation, the acid was formed by the reaction of sulfur trioxide (SO_3) with H_2O in different mixing ratios. This method of acid generation has been used widely for the generation of both aerosols and thin films.[12,13] Investigations of such films using infrared spectroscopic techniques have suggested that characteristic films can be identified and reproduced with relative ease by following experimental "recipes" with regard to temperature and the relative abundance of water. Horn et al.[14−16] have performed a comprehensive range of experiments, and phase transitions within the film have been observed using ATR-IR spectroscopy. Distinct spectra of the sulfuric acid, the monohydrate, SAM, and the tetrahydrate, SAT, films have been generated. Unfortunately, despite the inherently sensitive nature of the ATR application of FT-IR to the films the observed spectra are predominantly representative of the bulk species and not the exposed surface of the film.

The technique of static secondary ion mass spectrometry (SSIMS) provides information relating to the uppermost monolayers of the sample with very high chemical sensitivity. The application of the technique to atmospherically relevant samples has proven extremely useful in the investigation of the interaction of a variety of chlorine-containing species on ice surfaces.[17−19] The SSIMS experiment involves the removal and ionization of fragments of the surface using a focused high-energy ion beam to produce a mixture of predominantly neutral species along with positive and negative secondary ions. The ions can be extracted and analyzed using mass spectrometry. Despite being an inherently destructive technique, the sputtered material is considered to be representative of the original surface so long as the flux of the primary ion beam is minimized to remove less than 1% of the surface. For most samples, this implies a primary beam dose of less than 10^{13} impacts cm^{-2} of the sample, the so-called static limit.[20]

Experimental Section

The analysis was performed using a previously described[19] Kratos Prism series time-of-flight secondary ion mass spectrometer fitted with a Kratos Minibeam III ion gun to produce a primary ion beam of Ar^+ at 10 keV. Ultrahigh vacuum conditions were achieved and maintained by two turbomolecular pumps on the load chamber and flight tube and an ion pump on the main analysis chamber. Base pressures of 1×10^{-9} mbar are obtainable following an instrument bake. However, operating pressures closer to 1×10^{-8} mbar were recorded as a result of the reintroduction of water into the system and the presence of argon from the ion gun that is not efficiently removed from the chamber by the ion pump.

The sample stage/manipulator was manufactured by Kore Technology and features a hollow copper block onto which the sample stub is clamped. The sample is cooled by passing $N_2(g)$ through the copper block following passage through a liquid-nitrogen heat exchanger (approximately 4 m of $^1/_8$ in. copper

* Corresponding author. E-mail: john.vickerman@umist.ac.uk.
[†] UMIST.
[‡] University of Manchester.

10.1021/jp0372284 CCC: $27.50
Published on Web 04/15/2004

pipe suspended in a dewar of liquid nitrogen). The temperature is measured using a copper/constantan thermocouple attached to the stage in close proximity to the sample face and monitored using an Omega CN76000 temperature controller. The temperature is principally controlled by varying the flow of gas through the system, although the sample stage is also fitted with a filament for rapid heating.

Up to three gases can be introduced simultaneously into the vacuum chamber through precision leak valves. PTFE tubing carries the gases from the valves to the sample stage. Gases can be back-dosed into the chamber, or the sample stub can be swung away from the SIMS analysis position for direct dosing of gases onto the sample face.

Total and relative independent gas-pressure measurements were made using an ion gauge and a VG Micromass quadrupole residual gas analyzer (RGA). Ion gauge readings are quoted in millibars. RGA measurements use arbitrary units, although total pressure measurements using the RGA give pressures within 10% of those measured using the ion gauge. Exact pressures of SO_3 are not accurately known because of the difficulty in establishing relative sensitivity factors for the detection of the species by the quadrupole. (Relative sensitivity is a function of mass transmission and ionization efficiency.) However, the manufacturer's calibration of the RGA used in this study gives a predicted mass transmission of 0.35 for $m/z = 80$ relative to nitrogen; the relative ionization efficiency can be approximated to the known ion gauge sensitivity for SO_2 (2.1 relative to nitrogen). This gives a combined sensitivity of 1.36 relative to nitrogen. (Relative H_2O sensitivity is assumed to be unity.)

The films analyzed in this study were formed by the co-deposition of H_2O (purified by a Millipore Milli-Q water system) and anhydrous sulfur trioxide (Aldrich, 99%) directly onto a gold foil substrate attached to the sample stub and cooled to temperatures in the region of 200 K. At the temperatures and pressures used for the deposition, neither of the pure reactants should condense on the surface, only products formed by the reaction of the two species.

Horn et al.[15] reported the repeatable formation of a sulfuric acid monohydrate (SAM) film at temperatures ranging from 180 to 200 K by the co-deposition of SO_3 and H_2O.

Results and Discussion

The results presented detail the characterization, using ToF-SIMS, of sulfuric acid species present in the bulk and on the surface of the films. Trends in spectral features can be used to identify changes in film composition and provide evidence supporting the existence and surface localization of molecular hydrates.

ToF-SIMS spectra of sulfuric acid and the various hydrates thereof produce a series of easily identifiable peaks with many of the major fragments appearing in both a protonated and nonprotonated form as listed in Table 1. Charging effects were not observed on the samples; sulfuric acid hydrates may conduct electricity by proton switching, and charging is expected to be minimized by using thin samples such as those formed in this study. Following the methods of Horn et al.,[14,15] each experiment began with the deposition of a supposedly monohydrate film that could be analyzed and then subjected to changes in temperature and water pressure prior to subsequent analysis.

Attempts to acquire reproducible surface spectra representative of the sulfuric acid monohydrate, on a day to day basis, proved significantly more difficult than anticipated from reports of infrared characterization. The films formed were stable over several hours, but relative peak intensities showed variation beyond the error in reproducibility of the ToF-SIMS experiment.[21] The surface homogeneity of the films was assessed by acquiring spectra from different points on the sample surface; no significant variation was observed. However, separate domains may exist on the surface of the film that are not observed if they are below the resolution of the ion beam (spot size estimated to be between 250 and 500 μm^2), with an average surface spectrum being produced.

TABLE 1: Commonly Observed Ion Fragments in the Positive Ion Spectra of Sulfuric Acid and Hydrates Thereof

m/z	ion
18	H_2O^+
19	$H(H_2O)^+$
32	S^+
37	$H(H_2O)_2^+$
48	SO^+
49	HSO^+
65	HSO_2^+
98	$H_2SO_4^+$
99	$(H_2SO_4)H^+$
116	$H_2SO_4(H_2O)^+$
117	$H_2SO_4(H_2O)H^+$
135	$H_2SO_4(H_2O)_2H^+$
153	$H_2SO_4(H_2O)_3H^+$
197	$(H_2SO_4)_2H^+$

It was suggested that subtle changes in experimental conditions during film deposition (e.g., temperature of the laboratory and therefore the reactants) resulted in significant compositional changes in the uppermost surface layer(s) of the film despite the bulk deposition product consisting of the expected monohydrate. Initial ATR-IR experiments performed by Horn et al.[15] would show no significant spectral changes unless the deposited films were extremely thin, whereas the SIMS technique is inherently very surface sensitive, with 95% of the sputtered material originating from the top two monolayers of the sample.

However, the SIMS experiment allows the deposited film to be depth profiled to investigate compositional variation from the surface into the bulk. The ion beam is rastered over an area of the sample surface prior to the acquisition of a spectrum. The process is repeated several times following the removal of subsequent layers of material. Although quantitative depth measurements require knowing the sputter yield of the material under analysis (along with the raster area and ion beam current), qualitative data can be readily obtained provided conditions remain constant for each period of surface etching.

The etching process results in the exposure of the film to an ion dose far in excess of the static limit, and the bombardment of many sample materials, particularly complex organic molecules, with similar monatomic primary ions has been reported to show spectral changes as a result of surface damage where the loss of chemically characteristic fragment ions is observed. However, in contrast to organic materials, these films consist of small molecules, ions, and ionic clusters that may be less susceptible to bombardment-induced fragmentation. Thus, it is possible that damage effects are not observed because both the pristine and bombarded surfaces produce the same ions. A number of test profiles on approximately monohydrate films show very little spectral variation with ion dose, whereas an alteration of the H_2O/SO_3 mixing ratio during deposition produces films showing a clear distinction between surface and bulk regions of the film (e.g., Figure 4); thus, we are confident that the spectral changes observed during depth profiling reflect real changes in chemistry.

To explain variation in spectral features, peak area intensities are normalized relative to the $^{32}S^+$ peak in the same spectrum.

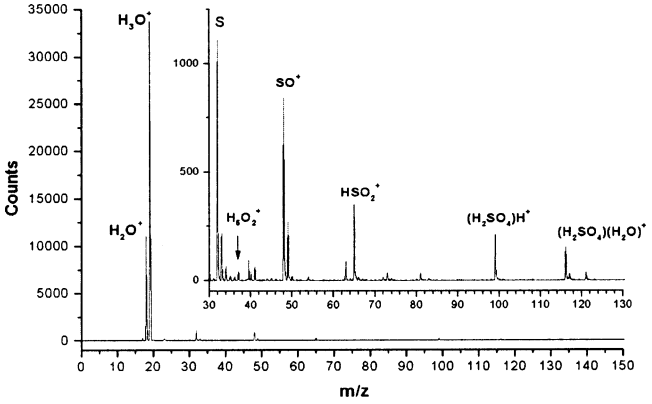

Figure 1. SIMS spectrum of bulk sulfuric acid monohydrate at 200 K deposited using 1×10^{-8} mbar H_2O and ca. 5×10^{-10} mbar SO_3.

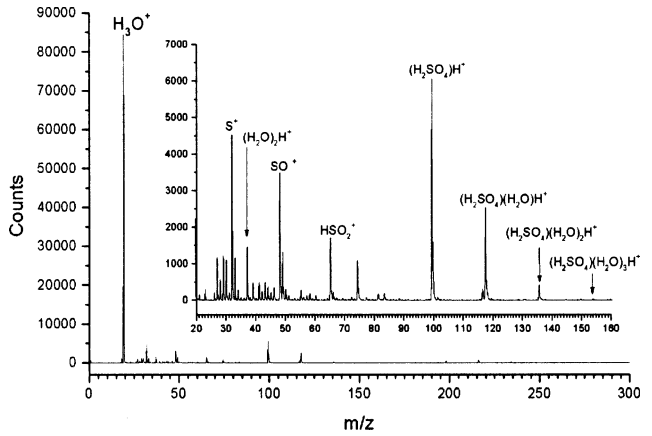

Figure 2. SIMS spectrum of surface sulfuric acid tetrahydrate (SAT) at 190 K following the exposure of a monohydrate film to ca. 1×10^{-6} mbar H_2O for 30 min.

Although the sulfur peak intensity changes with deposition conditions, it is present in all spectra as an ultimate fragment of the acid. The alternative of calculating intensities relative to total counts in the spectrum becomes less meaningful during depth profiling as the substrate is approached and signal is detected from interface contaminants, especially the alkali metals that give intense peaks due to their ionization efficiency.

Depth profiling a supposedly monohydrate film, deposited using 1×10^{-8} mbar H_2O and a range of SO_3 pressures at 200 K, showed definite variations between the surface and bulk. However, bulk spectra were reproducible, and we judge Figure 1 to be a representative spectrum of SAM. The ability to depth profile the samples also provides clear evidence that any surface species present on the film are not mobile in the time frame of the experiment.

SAM-to-SAT Conversion. The conversion of the monohydrate film to the tetrahydrate is observed routinely in the ATR-IR experiment following cooling of the sample under increased pressure of water. A SAM film presenting a spectrum similar to that in Figure 1 was cooled to 190 K under 1×10^{-6} mbar of H_2O for 15 min. The vacuum must be allowed to recover prior to the acquisition of spectra; therefore, the transition between the two hydrates could not be directly monitored. The spectrum in Figure 2 is that of the film 5 min after the H_2O addition. There is a significant increase in the intensities of H_3O^+ and $(H_2O)_2H^+$. The ratio of the $(H_2O)_2H^+$ peak to the $^{32}S^+$ has increased 3.4 times. The relative intensities of the SO^+ and HSO_2^+ peaks have also changed, although the ratio between SO^+ and HSO_2^+ remains constant.

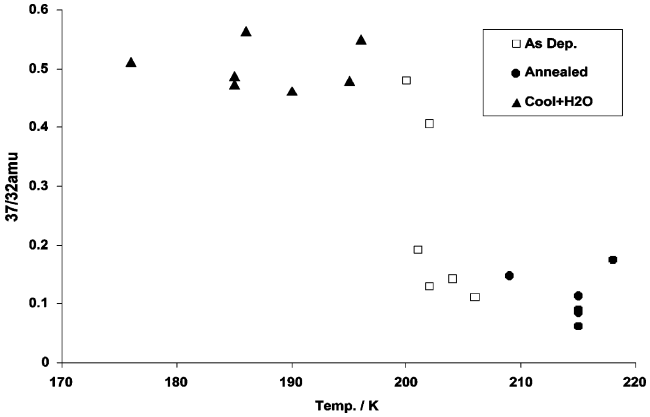

Figure 3. Variation of the ratio of $(H_2O)_2H^+$ ($m/z = 37$) to S^+ ($m/z = 32$) with temperature. Films are shown as deposited (using approximately 1×10^{-9} mbar H_2O and 4×10^{-10} mbar SO_3), annealed, and following exposure to H_2O at low temperatures.

The experiment was repeated many times, and as with the monohydrate films, general trends appear in relative peak intensities. Although it is difficult to produce films with identical spectral features, the observed transition seen in the $(H_2O)_2H^+$ to S^+ ratio upon cooling with the addition of H_2O is reliable. The variation in the $(H_2O)_2H^+/S^+$ ratio for these films with respect to temperature is displayed in Figure 3.

Two regimes are clearly visible along with a phase transition at around 200 K. Upon cooling a monohydrate under excess H_2O, a reproducible ratio of 0.5 is observed between the two peaks, indicating the formation of the tetrahydrate. Above 205 K, it becomes difficult to form films of any substantial thickness; however, once a monohydrate film has been deposited, it is stable to limited heating as shown by $(H_2O)_2H^+/S^+$ peak ratios of $\sim$0.12 for films annealed following deposition.

Depth profiles of sulfuric acid tetrahydrate films formed by this method show a constant $(H_2O)_2H^+/^{32}S^+$ ratio of 0.5 until the substrate is approached.

Characterization of Surface Species. Because the variation in surface composition was considered to be a result of subtle changes in deposition conditions that were difficult to control, it was necessary to gain at least qualitative information regarding spectral variations corresponding to changes in temperature and the SO_3/H_2O ratio. Recent literature provides possible explanations for the observed variation in surface chemical structure.

Molecular modeling and microwave spectroscopic studies have indicated the ability of sulfuric acid to form a number of stable compounds by the hydrogen bonding of a water molecule to the double-bonded oxygen atom and/or the oxygen-bound acidic hydrogen.[22−24] It is also suggested that the H_2O molecule can act as a bridge between acid molecules, leading to a range of complexes open to polymerization. The formation of the ionic monohydrate of sulfuric acid becomes more stable as the number of available water molecules is increased, so under water-deficient conditions, the formation of the hydrogen-bonded compounds is more reasonable. Vibrational sum frequency generation studies have also provided evidence for the presence of unionized species on the surface of low-temperature liquid sulfuric acid.[25] One such species, a sulfuric acid/water 1:1 complex with the H_2O molecule bridging the O and OH groups, gives predicted bond vibrations in good agreement with a species observed by Horn et al.[26] in a number of ATR-IR experiments. The species was most easily observed in the ATR-IR experiments where the films had been deposited under extremely H_2O-deficient conditions. Horn et al.[16] describe the relative mixing ratios of H_2O and SO_3 during deposition using the ratio of SO_3

to H_2O as measured using a nude ion gauge and designating it the "R_p value". The 1:1 complex was reported to represent the majority of the film in samples deposited close to 190 K with R_p values of 5 and 70. More recently, the same species has been observed in infrared spectra of aerosols at low temperatures and restricted water availability.[27]

In the course of this study, ToF-SIMS evidence supporting the existence of these species has been found, which also confirms that they are located on the surface of the acid hydrate films.

Low-Temperature H_2O-Deficient Films. Extremely H_2O deficient films have been produced in the ToF-SIMS instrument using conditions similar to those of Horn et al.[16] Films were deposited from 1×10^{-7} mbar H_2O with 5×10^{-7} mbar SO_3 for $R_p = 5$ and 7×10^{-6} mbar SO_3 for $R_p = 70$. The films were deposited and analyzed at 190 K with an additional experiment performed where the $R_p = 5$ film was deposited and analyzed at 200 K.

All peak areas in these spectra were substantially reduced relative to the $^{32}S^+$ peak compared with those previously deposited with lower SO_3 content. Depth profiling showed that as with the films containing less SO_3 there is still a distinction between the surface and bulk features of the acid film, although this was much less apparent on the 200 K film. However, all of the spectra including those of the bulk material contained predominantly the protonated $(H_2SO_4)(H_2O)H^+$ $m/z = 117$ peak with only a very small deprotonated peak at $m/z = 116$.

This study concludes that the 1:1 complex is characterized by a very high ratio of the $m/z = 117$ to 116 species.

Depth Profiling. We return to a consideration of the surface state of the monohydrate films. Depth profiling a supposedly monohydrate film, deposited using 1×10^{-8} mbar H_2O and 2×10^{-10} mbar SO_3 at 200 K, resulted in the following observations. The relative intensity of the H_3O^+ peak is approximately constant until the substrate is approached, where there is a sudden decrease in intensity. $(H_2O)_2H^+$ intensity is greatest at the film surface but quickly drops to a constant level. SO^+ and HSO_2^+ peaks show a direct correlation to each other, with the relative intensity of SO^+ being approximately 2.4 times that of HSO_2^+. There is a very small reduction in the intensities of these peaks from the topmost layers of the film to the bulk before a steady regime is reached. The $m/z = 116$, $(H_2SO_4)(H_2O)^+$ and $m/z = 117$, $(H_2SO_4)(H_2O)H^+$ intensities are both significantly stronger at the film surface, with the protonated form being dominant. Upon removal of the top layer of the films, the protonated ($m/z = 117$) peaks are reduced in relative intensity to give constant ratios of ~0.075 and ~0.1 relative to sulfur, with the unprotonated ($m/z = 116$) peaks now the more intense (Figure 4). The changes in the $(H_2SO_4)(H_2O)H^+$ intensity appear to be directly linked to those of the $(H_2SO_4)H^+$ peak, suggesting that the latter is a fragment of the former. Further amplifying these results, Figure 4 illustrates the relative changes in intensity of the $(H_2SO_4)(H_2O)H^+$ and $(H_2SO_4)(H_2O)^+$ peaks during the depth profiling of two films deposited at 200 K with 1×10^{-8} mbar H_2O, one film with 2.5×10^{-10} mbar SO_3 and the other with 4×10^{-10} mbar SO_3. The 4×10^{-10} mbar SO_3 film shows little variation between the surface and bulk, indicating a predominantly monohydrate interface; the 2.5×10^{-10} mbar SO_3 film, however, shows significantly increased surface signal for these species, particularly for the protonated form over the bulk SAM. It is clear that the surface of the film is sensitively dependent on the mixing ratio of H_2O and SO_3 during deposition and that the variations in the surface state can be followed by the variation in the relative intensities of several peaks, particularly those of the protonated water/sulfuric acid fragments exemplified by the $(H_2SO_4)(H_2O)H^+$ species at $m/z = 117$.

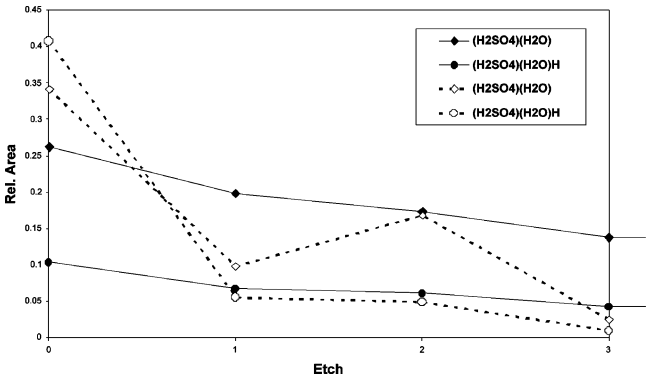

Figure 4. Variation of $(H_2SO_4)(H_2O)H^+$ and $(H_2SO_4)(H_2O)^+$ relative to $^{32}S^+$ as a function of depth for films deposited using 1×10^{-8} mbar H_2O with 2.5×10^{-10} (- - -) and 4 (—) $\times 10^{-10}$ mbar SO_3 at 200 K.

Effect of Deposition Temperature (and SO_3/H_2O Variation). To describe the effect of the temperature changes and variation in H_2O availability during deposition, it is easiest to present a number of plots of the relative peak intensities to illustrate a series of trends in the spectra.

Spectra were recorded of the surfaces of films deposited with constant H_2O and varying amounts of SO_3 over temperatures from 180 to 205 K. Assigning spectral changes to small variations in relative pressures can be done with confidence only by performing experiments in which the majority of variation results from the adjustment of a single parameter. SO_3 pressures corresponding to RGA readings of 2.5×10^{-10}, 5.0×10^{-10}, and 10×10^{-10} mbar were used in conjunction with temperature variations of approximately 5 K. The error in reproducibility of the ToF-SIMS analyses are expected to be much less than 5% [21] and insignificant compared to the reproducibility of film-deposition conditions. Calculations of surface-spectra reproducibility following deposition give errors of $<\pm 3\%$ for the intensities of the SO^+ and HSO^+ peaks relative to sulfur but with much larger errors (approximately $\pm 25\%$) for $(H_2SO_4)(H_2O)H^+$ and $(H_2SO_4)H^+$. However, the adjustment of deposition conditions in this study produces trends beyond this experimental error.

Plots of many of the major fragments observed in the spectra show three clear temperature regions (Figures 5−9). A stable region with little change in peak intensity with respect to either temperature or SO_3 concentration during deposition is evident in the temperature range from 185−195 K. Below 185 K, there is also a consistent feature of increased relative peak intensity of the water-containing fragments (with the exception of the H_2O^+ peak). At 205 K, there is a further change in the relative peak intensities of all of the fragments except the H_3O^+.

The H_3O^+ peak on films deposited at 205 K shows an expected increase with decreasing SO_3 concentration (increased H_2O availability) during deposition (Figure 5). At deposition temperatures ranging from 205 to 185 K, the peak intensity relative to sulfur is approximately constant. At 180 K, there is a sharp increase in the relative peak intensity of this fragment (the SO_3-deficient film displaying the greatest relative intensity); this indicates either the formation a new surface species that is stabilized at this lower temperature or the possible formation of ice on the surface. At 180 K, the SO_3/H_2O ratio during film deposition has little if any effect on the relative peak intensity.

The $H_5O_2^+$ peak shows a comparable temperature variation to that previously illustrated in the conversion of SAM to SAT.

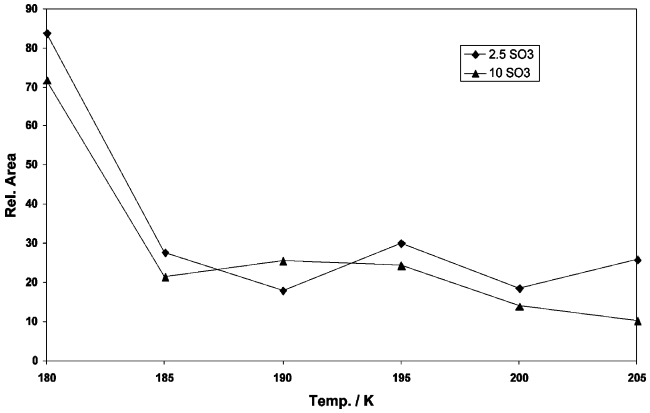

Figure 5. Variation of the H_3O^+ peak relative to $^{32}S^+$ in films deposited using 1×10^{-8} mbar H_2O with 2.5×10^{-10} and 10×10^{-10} mbar SO_3 over temperature.

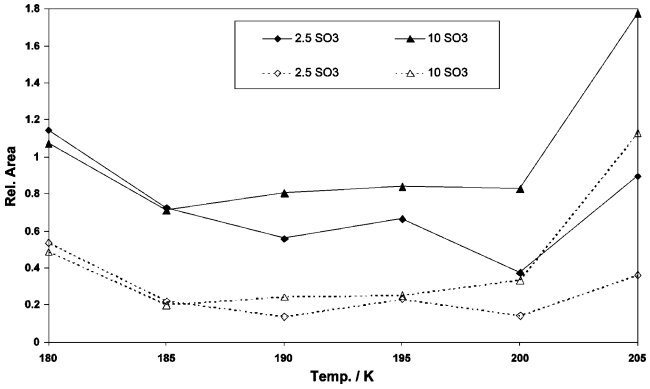

Figure 6. Variation in the relative intensity of sulfur of the SO^+ (—) and HSO_2^+ (- - -) peaks in films deposited using 1×10^{-8} mbar H_2O with 2.5×10^{-10} and 10×10^{-10} mbar SO_3 over temperature.

This peak varies in a similar manner with respect to water availability during deposition to that observed for the H_3O^+ peak, as one might expect for two protonated water species. Again, the film deposited at 205 K shows increasing peak intensity with increasing water availability, but in the temperature range of 185 to 195 K, it is the 10×10^{-10} mbar SO_3 film that gives the greatest relative intensity. At 180 K, there is a return to H_3O^+-like behavior.

At 205 K, the relative abundance of SO^+ and HSO_2^+ (Figure 6) increases as the SO_3 concentration increases from 2.5×10^{-10} to 10×10^{-10} mbar. The SO^+ and HSO_2^+ peaks show a directly proportional relationship to each other, with $SO/HSO_2 \approx 2.5$ in agreement with that of the bulk SAM films observed in the depth profile. The variation of these peaks with respect to changing SO_3 concentration during deposition is much greater at higher temperature, with the 2.5×10^{-10} and 10×10^{-10} mbar SO_3 films producing peaks with approximately equal intensities relative to sulfur at 180 and 185 K. There is variation in the proportionality constant between the two relative peak areas at deposition temperatures below 200 K, with a general increase in the value ($\sim$3.5 at 185, 190, and 195 K). The increase in relative peak intensity is again observed at 185 K, and as with the H_3O^+ peak, there is no clearly apparent dependence on water/SO_3 availability during deposition. These trends continue to indicate the presence of three separate surface species.

The change in the peak area of the $(H_2SO_4)(H_2O)^+$ fragment (relative to $^{32}S^+$) is illustrated in Figure 7 and shows a general trend similar to that observed for the $(H)SO_x^+$ fragments with increasing intensity at the two extremes of deposition temperature. Also apparent for this peak is an inversion in the effect of SO_3 concentration during deposition. Films deposited above 200 K display a large increase in relative peak intensity with increased SO_3 availability during film formation, whereas below 200 K it is the 2.5×10^{-10} mbar SO_3 (water-rich) films that result in the greatest relative peak intensities.

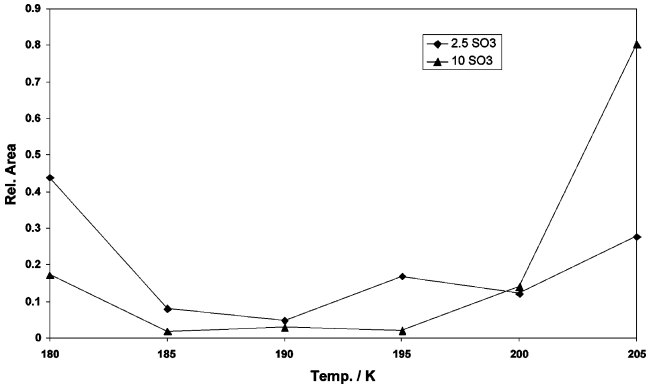

Figure 7. Variation in intensity of the $(H_2SO_4)(H_2O)^+$ peak relative to $^{32}S^+$ in films deposited using 1×10^{-8} mbar H_2O with 2.5×10^{-10} and 10×10^{-10} mbar SO_3 over temperature.

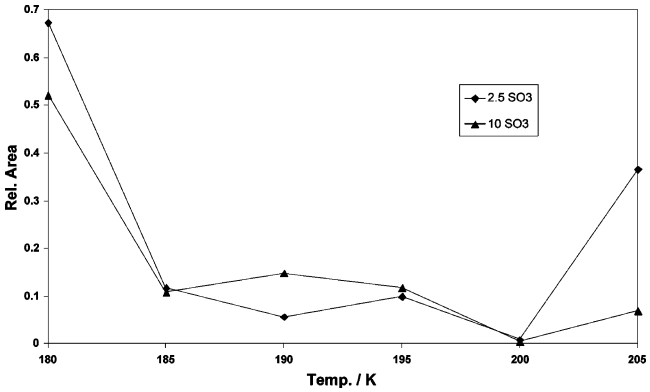

Figure 8. Change in relative intensity of sulfur of the $(H_2SO_4)(H_2O)$-H^+ peak deposited using 1×10^{-8} mbar H_2O with 2.5×10^{-10} and 10×10^{-10} mbar SO_3 over temperature.

It is apparent that the nature and composition of the surface species of these thin films are influenced greatly by both the relative H_2O availability and temperature, with equivalent mixing ratios of H_2O and SO_3 resulting in complex spectral variation as the temperature of deposition is adjusted. The protonated $(H_2SO_4)(H_2O)H^+$ $m/z = 117$ ion (Figure 4) is observed at 200 K under low SO_3 deposition conditions as a predominantly surface-residing species. This $m/z = 117$ peak has been shown to increase in relative intensity at 205 K as a result of increased H_2O availability during deposition. Conversely, below 200 K there is little obvious dependence of relative peak area on SO_3 concentration during deposition. The stable region between 185 and 195 K is evident, as is the increase in relative peak intensity at 180 K (Figure 8). As observed during the depth profile experiments, the $(H_2SO_4)H^+$ fragment demonstrates a proportional relationship to the $(H_2SO_4)(H_2O)H^+$ fragment, indicating one to be a fragment of the other. Because films at 205 K show an increase in all protonated water-containing species under lower SO_3 (higher relative H_2O) deposition conditions, it seems reasonable to assume that at this temperature the water is behaving as a proton acceptor for the acid (although the H_2O is the only source for additional hydrogen atoms during deposition). The extra water is localized on the surface but does not act as a liquid solvent, rather existing

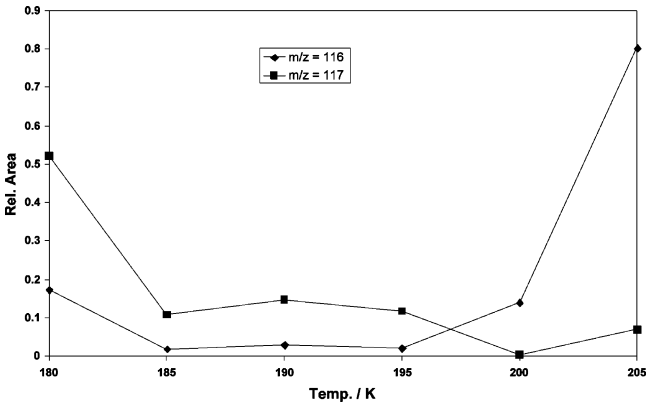

Figure 9. Change in intensity of the $(H_2SO_4)(H_2O)^+$ and $(H_2SO_4)(H_2O)H^+$ peaks relative to $^{32}S^+$ in films deposited using 1×10^{-8} mbar H_2O and 10×10^{-10} mbar SO_3 with varying deposition temperature.

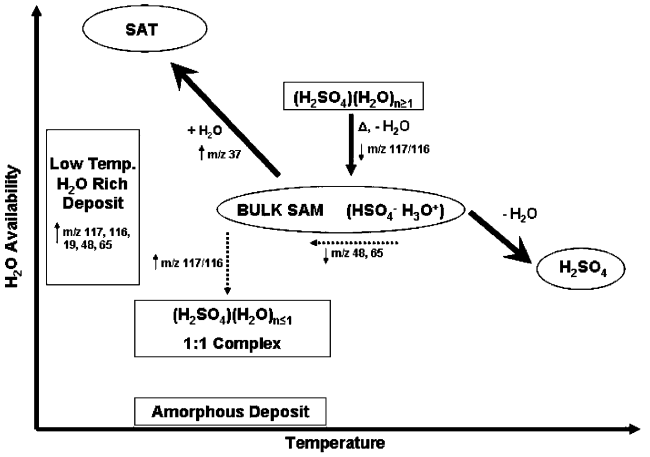

Figure 10. Schematic of suggested deposition products illustrated with respect to temperature and water availability during deposition; trends in relative peak intensity are also included. Bold arrows indicate experimentally observed interconversions; broken arrows illustrate the direction of the labeled changes in peak intensity.

as a solid layer as demonstrated by the ability to depth profile through such films.

The increase in the relative intensity of this $m/z = 117$ peak under H_2O-deficient conditions below 185 K cannot be as easily explained. Here the increase must arise from the formation of a new surface species.

Figure 9 illustrates clear transitions in the surface composition as monitored by the $H_2SO_4(H_2O)$ species as a result of changing deposition temperature. As with the majority of the other plots of fragment intensity, the overall increase in intensity is observed at the two extremes of deposition temperature. Here it is also clear that the deprotonated species $m/z = 116$ becomes the favored ion at 200 K, a feature that is further enhanced as the deposition temperature is increased to 205 K. The 185−195 K region of the plot shows the steady regime observed for all of the major fragments of the mass spectrum indicating the formation of the stable surface complex. Again a further transition is observed at 180 K, where the low temperature facilitates the incorporation and stabilization of additional water in the film.

On the basis of the ToF-SIMS results, we suggest the following model of the sulfuric acid film surfaces illustrated in Figure 10.

A stable species is observed on the surface of films formed between 185 and 195 K and is considered to be the approximately 1:1 acid/water complex recently reported by Horn et al. and represented in Figure 10 as $(H_2SO_4)(H_2O)_{n\leq1}$. This species is observed in the bulk form for extremely low water content films as indicated by the presence of the $m/z = 117$ peak and very little or none of the corresponding $m/z = 116$ and is illustrated in the figure as an amorphous deposit.

At deposition temperatures of 200 and 205 K, increased H_2O availability during deposition produces a surface-localized species, again with the high $m/z = 117/116$ ratio, $(H_2SO_4)(H_2O)_{n\geq1}$. These spectral observations may be explained as a result of protonation of the water by the acid at the surface but also as the formation of another molecular species, possibly a mixture of 1:1 and 1:2 acid/water species. The bulk film underlying each of these surface species is considered to be monohydrate in character.

The transformation of the monohydrate to the tetrahydrate upon cooling under additional H_2O, monitored by the change in intensity of the $m/z = 37$ ($H_5O_2^+$) relative to $^{32}S^+$, has been described previously in this paper and is also included in Figure 10. Deposition at low temperatures results in the formation of H_2O-rich films as ice nucleation temperatures are approached.

The ultimate dehydration product upon warming these films is molecular sulfuric acid (H_2SO_4).

Conclusions and Atmospheric Implications

Sulfuric acid-based films, formed by the co-deposition of H_2O and SO_3, can be analyzed readily using ToF-SIMS to produce spectra containing characteristic mass fragments. Changes in the relative intensities of these have been shown to be indicative of the temperature at which the film was deposited and the mixing ratio of the reactant species. ToF-SIMS spectra characteristic of the bulk mono- and tetrahydrates have been obtained using the preparation protocols defined by Horn et al.[15−17]

The surface sensitivity of the ToF-SIMS technique coupled to the ability to depth profile the samples has clearly illustrated the existence of separate surface species on a wide range of films.

On the basis of the observations, a number of distinct surface species have been suggested relating to observations in previous infrared studies and molecular modeling predictions.

Although the nature of the SIMS experiment does not allow species to be analyzed at atmospheric pressure, this study further indicates the complexity of the nucleation process of sulfuric acid species and shows a clear distinction between bulk and surface regions of the deposits. This variation is commensurate with the prediction and infrared observation of molecular hydrates on sulfuric acid aerosols and on the surface of thin films. There are obvious implications for atmospheric models concerned with reaction on and in atmospheric aerosols, further demonstrating the need for an increased mechanistic understanding of these atmospherically relevant reactions.

Acknowledgment. This work was funded by the U.K. Natural Environmental Research Council. We thank Sue Couling for valued discussion of her results.

References and Notes

(1) Solomon, S. *Nature* **1990**, *347*, 347−354.
(2) Rodriguez, J. M. *Science* **1993**, *261*, 1128.
(3) Hofmann, D. J.; Oltmans, S. J.; Harris, J. M.; Solomon, S.; Deshler, T.; Johnson, B. J. *Nature* **1992**, *359*, 283−287.
(4) Farman, J. C.; Gardiner, B. G.; Shanklin, J. D. *Nature* **1985**, *315*, 207−210.
(5) Dentener, F. J.; Crutzen, P. J. *J. Geophys. Res.* **1993**, *98*, 7149.
(6) Toon, O. B.; Tolbert, M. A. *Nature* **1995**, *375*, 218−221.
(7) Heathfield, E.; Newman, D. A.; Ballard, J.; Grainger, R. G.; Lambert, A. *Appl. Opt.* **1999**, *38*, 6408.

(8) Iraci, L. T.; Middlebrook, A. M.; Wilson, M. A.; Tolbert, M. A. *Geophys. Res. Lett.* **1994**, *21*, 867.

(9) Schindler, L. R.; Roberts, J. T. *J. Phys. Chem.* **1996**, *100*, 100, 19582−19586.

(10) Martin, S. T.; Salcedo, D.; Molina, L. T.; Molina, M. J. *J. Phys. Chem. B* **1997**, *101*), 5307−5313.

(11) Bertram, K.; Patterson, D. D.; Sloan, J. J. *J. Phys. Chem.* **1995**, *100*, 2376.

(12) Nash, K. L.; Heathfield, A. E.; Newman, D. A.; Horn, A. B. *Phys. Chem. Chem. Phys.* **2002**, *4*, 2539−2545.

(13) Kane, S. M.; Caloz, F.; Leu, M.-T. *J. Phys. Chem. A* **2001**, *105*, 6465−6470.

(14) Horn, A. B.; Sully, K. J. *Phys. Chem. Chem. Phys.* **1999**, *1*, 3801−3806.

(15) Nash, K. L.; Sully, K. J.; Horn, A. B. *Phys. Chem. Chem. Phys.* **2000**, *2*, 4933−4940.

(16) Couling, S. B.; Sully, K. J.; Horn, A. B. *J. Am. Chem. Soc.* **2003**, *125*, 1994.

(17) Donsig, H. A.; Vickerman, J. C. *J. Chem. Soc., Faraday Trans.* **1997**, *93*, 2755−2761.

(18) Donsig, H. A.; Herridge, D.; Vickerman, J. C. *J. Phys. Chem. A* **1999**, *103*, 9211−9220.

(19) Donsig, H. A.; Herridge, D.; Vickerman, J. C. *J. Phys. Chem. A* **1997**, *102*, 2302−2308.

(20) *ToF-SIMS Surface Analysis by Mass Spectrometry*; Vickerman, J. C., Briggs, D., Eds.; Surface Spectra; I M Publications: Manchester and Chichester, UK, 2001.

(21) Gilmore, I. S.; Seah, M. P. *Surf. Interface Anal.* **2000**, *29*, 624−637.

(22) Bandy, A. R.; Ianni, J. C. *J. Phys. Chem. A* **1998**, *102*, 6533−6539.

(23) Ianni, J. C.; Bandy, A. R. *J. Mol. Struct: THEOCHEM* **2000**, *497*, 19−37.

(24) Fiacco, D. L.; Hunt, S. W.; Leopold, K. R. *J. Am. Chem. Soc.* **2002**, *124*, 4504−4511.

(25) Schnitzer, C.; Baldelli, S.; Shultz, M. J. *Chem. Phys. Lett.* **1999**, *313*, 416−420.

(26) Couling, S. B.; Nash, K. L.; Fletcher, J.; Henderson, A.; Vickerman, J. C.; Horn, A. B. *J. Am. Chem. Soc.* **2003**, *125*, 13038−13039.

(27) Couling, S. B.; Fletcher, J.; Horn, A. B.; Newnham, D. A.; McPheat, R. A.; Williams, R. G. *Phys. Chem. Chem. Phys.* **2003**, *5*, 4108−4113.